J Solid State Electrochem (2010) 14:2225–2233
DOI 10.1007/s10008-010-1055-3

ORIGINAL PAPER

Magnetic properties of nanocrystalline CoPt electrodeposited films. Influence of P incorporation

Meritxell Cortés · Elvira Gómez · Elisa Vallés

Received: 18 January 2010 / Revised: 15 March 2010 / Accepted: 16 March 2010 / Published online: 14 April 2010
© Springer-Verlag 2010

Abstract Platinum-rich CoPt films have been electrodeposited with the aim of preparing hard magnetic films on silicon-based substrates without the need for subsequent annealing. Electrodeposition conditions have permitted the crystalline structure of the films to be controlled. Pt percentages of up to 60–65 wt.% have been attained while maintaining the hexagonal Co phase, leading to CoPt films with moderate coercivity and good corrosion resistance. However, when low deposition potentials were used, CoPt films with higher Pt percentages were obtained, but in this case, the films exhibited an fcc structure, having lower coercivity and less corrosion resistance. The presence of hypophosphite in the solution limited the platinum percentage in the deposited CoPtP films, but an hexagonal close-packed (hcp) structure was always observed in this case. The incorporation of P into the deposits led to increases in both the coercivity of the films and the corrosion resistance of the coatings, with respect to pure CoPt. The highest coercivity was obtained for hcp CoPtP deposits with 40 wt.% of Pt.

Keywords Electrodeposition · Magnetic films · Cobalt–platinum–phosphorous alloy · X-ray diffraction · Corrosion resistance

M. Cortés · E. Gómez · E. Vallés (✉)
Electrodep, Departament de Química Física and Institut de Nanociència i Nanotecnologia (IN2UB),
Universitat de Barcelona,
Martí i Franquès 1,
08028 Barcelona, Spain
e-mail: e.valles@ub.edu

Introduction

Microelectromechanical systems (MEMS) are the integration of mechanical elements, sensors, actuators, and electronics on a substrate, commonly silicon, through microfabrication technology. Recently, there has been growing interest in how magnetic materials could be incorporated into MEMS devices for sensors or actuator applications. Electrochemical methods can be used in order to prepare magnetic materials compatible with MEMS processing. Electrodeposition has several advantages over other techniques, including the low cost and simplicity of the experimental setup, not requiring high temperatures or vacuum conditions. Moreover, it permits easy control of the growth process, film thickness, and chemical composition of the layer. Additionally, electrochemistry is fully compatible with microfabrication processes and has been used to prepare several micron-thick deposits of metals, alloys, and compounds on various substrates.

In our laboratory, soft magnetic layers of CoNi have been prepared by electrodeposition over silicon/seed layer substrates and incorporated as mobile elements in microvalves [1]. Although most of the magnetic microactuators developed by different researchers use soft magnetic materials [2–4], hard magnetic materials are also desirable in some applications (microsized motors, minipumps, microactuators) [5, 6]. The preparation of hard magnetic deposits by different techniques for MEMS magnetic actuators has recently been studied [7–14]. In this paper, we investigate how electrochemical deposition of microscale permanent magnets can be achieved for implementation in microactuators devices. The incorporation of ferromagnetic particles into a CoNi alloy matrix by means of electrodeposition has been studied as a way of preparing

hard magnetic films [15]. Another possibility is the direct electrodeposition of hard magnetic films over the silicon/seed-layer substrate. The most common hard magnetic materials are CoPt, FePt, and rare earths as $Nd_2Fe_{14}B$ or $SmCo_5$ [16–18], although the codeposition of rare earth magnetic thin films implies the use of organic solvents and the application of high negative potentials. Co-based alloys, such as CoNiP [7, 14, 19], CoP [20], CoPt [21–23], or CoPtP [20, 24–26], have been electrodeposited, resulting in high coercivity films. In these studies, a subsequent annealing step after following deposition is usually necessary in order to obtain the desired hard magnetic response. In our previous work, solutions for simultaneous deposition of Co, Pt, and P were tested [27].

Here, we report the preparation of platinum-rich CoPt films in order to obtain hard magnetic films deposited on silicon/seed-layer substrates without the need for subsequent annealing of the deposited films. High Pt percentages were desired for enhancing the magnetic anisotropy of the cobalt phase. Different deposition conditions will be characterized in order to obtain films with a composition and structure optimized for maximum coercivity, maximum permeability, and good corrosion resistance, desirable properties for use in magnetic microdevices. The influence of the P incorporation in the magnetic, structural, morphological, and corrosion-resistant properties of the CoPt electrodeposits, as well as the analysis of the changes in the deposition process and in the deposition rate, will be performed.

Experimental

Solutions containing $CoCl_2$, Na_2PtCl_6, boric acid, and NH_4Cl, all of analytical grade, were used to perform the CoPt electrodeposition in a three-electrode cell with control of the temperature. A solution containing 2.5×10^{-3}M $CoCl_2$+1.2×10^{-3}M Na_2PtCl_6+1 M NH_4Cl+30 gdm^{-3} H_3BO_3 was mainly used, although for some experiments the $[Na_2PtCl_6]/[CoCl_2]$ was decreased. Solutions were deaerated by argon bubbling before each experiment and then maintained under argon atmosphere. Sodium hypophosphite (10^{-2}M NaH_2PO_2) was used to induce phosphorous incorporation into some deposits. The pH of the solutions was adjusted to 4.5 to simultaneously avoid the precipitation of platinum oxides and the excessive evolution of hydrogen. Different temperatures (25 °C, 40 °C) have been tested. Stirring of the solution (60, 1,100 rpm) was maintained during the electrodeposition to assure a constant composition throughout the deposits.

A microcomputer-controlled potentiostat/galvanostat Autolab with PGSTAT30 equipment and GPES software was used for deposits preparation over silicon/Ti (1,000 Å)/Ni (500 Å) substrates (supplied by IMB-CNM.CSIC). These substrates were cleaned with acetone and ethanol and rinsed in water before deposition. The reference electrode was an Ag/AgCl/1-mol dm^{-3} NaCl electrode. All potentials were referred to this electrode. The counter electrode was a platinum spiral.

Corrosion test was carried out at 25 °C in a 5% NaCl (p.a.) solution. The films on 0.3-cm^2 silicon-based substrates were immersed in NaCl media for 3 h in order to determine the steady-state potential (E_{ss}). Immediately afterward, a linear potentiodynamic sweep between ±300 mV/E_{ss} was performed at 0.1 mV s^{-1} to find out corrosion potential (E_{corr}) and corrosion current density (j_{corr}). Nonstirring conditions were used during both polarization and potentiodynamic scan.

Leica Stereoscan S-360 and Hitachi H-4100FE scanning electron microscopes (SEM) were used to analyze deposits composition and for morphology observation, respectively. Structure of deposits were studied by means of a Philips MRD diffractometer with parallel optical geometry using Cu $K\alpha$ radiation (λ=0.1542 nm) and a texture goniometer that allows control of the sample rotation about the three axes.

Magnetic properties were characterized by means of a SQUID magnetometer at room temperature. Thicknesses of the coatings were measured using a Zygo NEW VIEW 100 white-light interferometer.

Results and discussion

Deposits preparation

Films were prepared potentiostatically or galvanostatically. Figure 1 shows representative transients corresponding to the electrodeposition. Potentiostatic curves obtained under stirring conditions showed (Fig. 1a, b) monotonic growth of the current density with time. Similar deposition rate was obtained at fixed potential in the presence or in absence of the hypophosphite in solution (in the range 500–700 nm/h). However, clear differences in the Pt percentage of the films were observed: Pt percentage decreased from 59.6 wt.% from free-hypophosphite bath to 38.7 wt.% Pt in the solution containing hypophosphite, and a 3.3 wt.% in P was detected.

When the galvanostatic technique was used, very negative potential values were attained to induce nucleation of the metals (nucleation spike). Subsequent stabilization of the potential occurred at longer deposition times, corresponding to the growth of the deposit over the initial nuclei formed. By comparing the $E-t$ transients recorded at the same current density (−4 mA cm^{-2}; Fig. 1c), less negative stabilization potentials were observed for CoPt

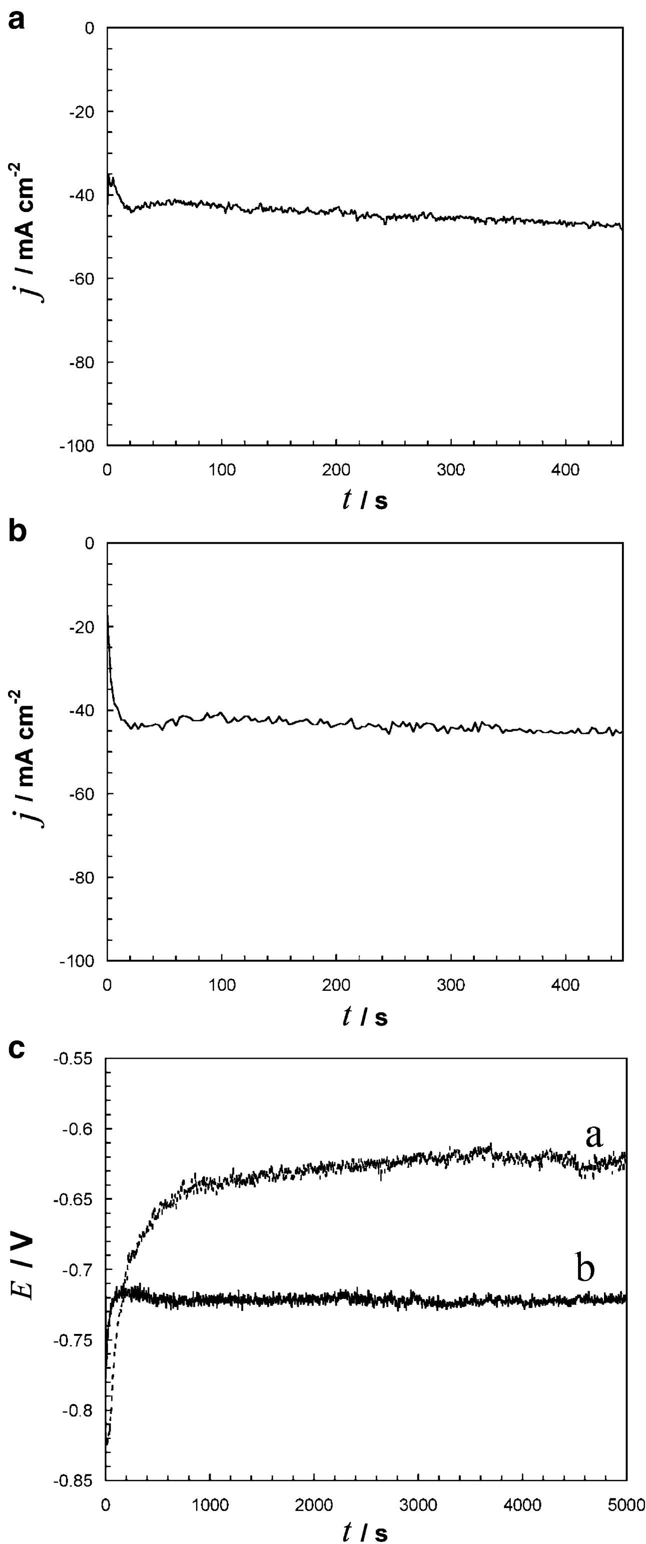

Fig. 1 Potentiostatic curves at −950 mV of a bath containing 2.5×10^{-3}M $CoCl_2$+1.2×10^{-3}M Na_2PtCl_6+1 M NH_4Cl+30 gdm^{-3} H_3BO_3. **a** Without hypophosphite, **b** with 10^{-2}M NaH_2PO_2. **c** Galvanostatic curves at −4 mA cm^{-2} of *a* the same solution as **a**, *b* the same solution than **b**. T=40 °C. ω=60 rpm

deposition (Fig. 1c, curve a) leading to platinum-rich CoPt deposits (77.4 wt.% Pt). For the same applied current density, more negative potentials were necessary to maintain the electrodeposition in the presence of phosphorous compound (Fig. 1c, curve b), and as a consequence, more cobalt-rich deposits were obtained (56 wt.% Co, 3 wt.% P). In the absence of hypophosphite, wide nucleation spike was obtained due to the significant simultaneous hydrogen evolution during platinum formation, which makes slow the nucleation process. Several authors have detected the capability of adsorption of hypophosphite anion over several metals as Ni, Co, Pd, and Pt [28–31]. Then, in the presence of hypophosphite, its adsorption over the first nuclei shifts both electrodeposition process and hydrogen evolution to more negative potentials. Then, growth of the deposit takes place at more negative potentials, and cobalt percentage in the deposits increased.

CoPt films

The CoPt films prepared were rich in platinum (Table 1). At one fixed deposition potential, composition has low temperature dependence, so 40 °C was selected as preparation temperature in order to attain higher deposition rates. For high deposition charge, it was possible to maintain a nearly constant composition, avoiding the decrease of the Pt percentage by providing a vigorous stirring to the solution (1,100 rpm) which permitted the removal of the evolved hydrogen present. After increasing the Co/Pt ratio, high cobalt content was detected in the deposits.

Deposits with nanometric thickness (<1 μm) containing 60–65 wt.% Pt were very smooth and reflective. Morphological analysis made by FE-SEM showed that they were formed by polyhedral fine grains (Fig. 2a). More compact and uniform deposits with smaller grain sizes were obtained for CoPt deposits by increasing the deposition charge, attaining micrometric thickness of the films (Fig. 2b), probably as a consequence of that the higher stirring rate used in these conditions favor both electroactive species approach and simultaneous hydrogen detachment. The observed morphology is characteristic of cobalt deposits showing hexagonal close-packed (hcp) structure [32]. The X-ray diffractograms of these CoPt deposits showed, next to some peaks corresponding to the substrate (*), diffraction peaks assigned to an hcp phase (Fig. 3a). However, the high incorporation of Pt in the deposits led to an hcp structure very distorted respect to that corresponding to pure hcp Co. The diffraction peak positions corresponding to the hcp phase shifted to lower 2θ values, indicating that platinum incorporation leads to greater lattice spacing with respect to the pure hcp cobalt phase. Using the DICVOL04 indexation program [33], the cell parameters of the hexagonal phase

Table 1 Composition of CoPt deposits prepared in different conditions

Sample	$-E$ (mV)	$-j$ (mA cm^{-2})	Stirring (rpm)	$-Q$ (C cm^{-2})	T (°C)	wt.% Co	wt.% Pt
A1[a]	950		60	20	40	40.4	59.6
A2[a]	950		60	20	25	35.1	64.9
A3[a]	950		60	30	40	37.4	62.6
A4[a]	950		1,100	190	40	41.4	58.6
A5[a]	950		1,100	276	40	39.6	60.4
A6[a]		4	60	20	40	22.6	77.4
A7[a]		4	60	67	40	20.6	79.4
B1[b]	950		60	20	40	60.9	39.1

[a] 2.5×10^{-3} M $CoCl_2$+1.2×10^{-3} M Na_2PtCl_6+1 M NH_4Cl+30 g dm^{-3} H_3BO_3 solution

[b] 5×10^{-3} M $CoCl_2$+1×10^{-3} M Na_2PtCl_6+1 M NH_4Cl+30 g dm^{-3} H_3BO_3 solution

were within the range of a=0.260–0.261 nm and c=0.422–0.424 nm corresponding to a cell volume (V) of 0.0247–0.0250 nm^3. From the broadening of the peaks, one can estimate the crystalline size domains using the Debye–Scherrer formula [34]. From the full width at half maximum values of the diffraction peaks corresponding to the 100 and 002 reflections and taking into account the instrumental linewidth, the estimated value of the crystalline domains was in the range of 20–25 nm, as corresponds to a nanocrystalline material.

These deposits showed coercivity values around 700 Oe and a high value of the M/H slope, revealing high permeability of the films (Fig. 3b). The incorporation of significant proportion of Pt in the hcp phase of Co led to a drastic increase of the coercivity of the films with respect to pure Co films [35] due to the high anisotropy induced. Higher Pt percentages in the deposits (>70 wt.%) were obtained applying low current densities (−4 mA cm^{-2}) as corresponds to the low stabilization potential attained (−600 mV). These platinum-rich layers showed nodular morphology (Fig. 4a) with around 100 nm of grain size. No polyhedral morphology was observed and a drastic decrease of the coercivity value was observed (Fig. 4b), probably as a consequence of a structural changes, no longer being the hexagonal phase. Actually, the XRD of these deposits showed that close to the peaks corresponding to the substrate, wide peaks assigned to the layer, revealing the nanometric size of the crystalline domains in the CoPt electrodeposits. An fcc phase was observed instead of an hexagonal one, as a consequence of the increase on Pt percentage (Fig. 4c), justifying the drastic different magnetic behavior of the coatings. For the fcc phase, the cell parameter estimated for CoPt deposits of 77 wt.% Pt was a=0.380 nm and the cell volume (V) was 0.0549 nm^3. A significant decrease of the crystalline domains was detected from the CoPt hcp to CoPt fcc phase due to Scherrer estimation led to a 7-nm value.

Corrosion experiments were carried out in order to evaluate whether the corrosion resistance was sensitive to the structure and morphology of the prepared CoPt deposits. Figure 5 shows the potentiodynamic polarization curves corresponding to different CoPt deposits. This figure indicates that hcp CoPt samples (B1, curve a and A1, curve b) show better corrosion resistance than the fcc CoPt (sample A6, curve c) because the corrosion potential values (E_{corr}) were more positive for CoPt deposits of hcp structure than for that presenting fcc structure. Moreover, for hcp CoPt coatings, the corrosion potential moved positively with increasing Pt content in the deposits (sample B1 39.1 wt.% Pt, sample A1 59.6 wt.% Pt). Higher j_{corr} was obtained for deposits with the fcc structure, corresponding to a higher corrosion rate (Table 2). A clear relation between composition, morphology, crystalline structure,

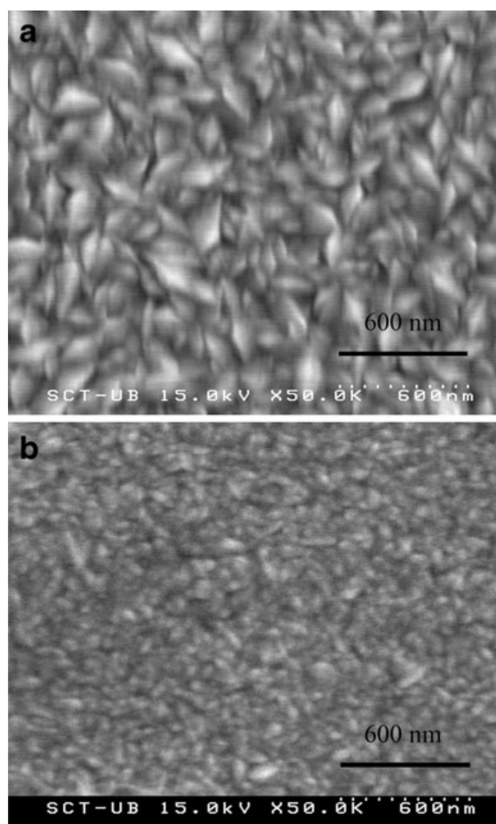

Fig. 2 FE-SEM images of CoPt deposits obtained from the solution of Fig. 1 at −950 mV. **a** Sample A3, thickness 180 nm, **b** sample A5, thickness 1.5 µm

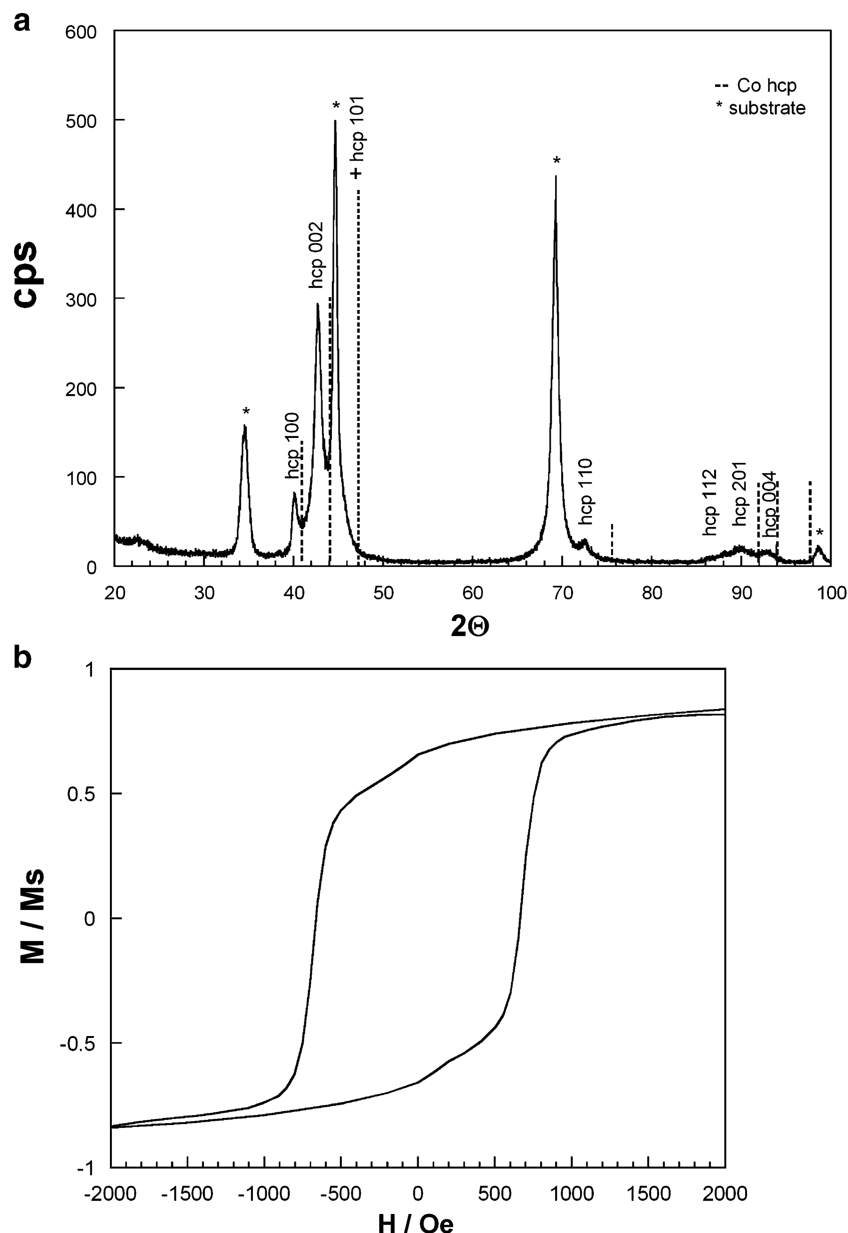

Fig. 3 **a** X-ray diffractogram of a CoPt deposit of 150 nm (sample A1), **b** normalized room temperature magnetization curve taken with the applied field parallel for a CoPt deposit of 150 nm (sample A2)

magnetic behavior, and corrosion resistance was observed for the CoPt prepared electrodeposits from the selected solution. CoPt hexagonal films showing polyhedral morphology presented more accused hard magnetic behavior and better corrosion resistance.

Influence of P in CoPt deposits

For the deposits prepared from the solution containing hypophosphite, P was moderately incorporated while Pt percentage decreased (Table 3). A limit in the Pt percentage in the ternary deposits was observed in the presence of hypophosphite because no more of 45 wt.% was obtained, while 60–65 wt.% was obtained from the same solution but in the absence of hypophosphite. For the ternary CoPtP deposition, it was difficult to maintain the deposits composition for high deposition charges, even under vigorous stirring conditions of the solution. A decrease of P incorporation was observed by increasing significantly deposition charge. Moreover, a higher increase of the deposition charge led to a decrease in Pt percentage in the deposits (Table 3). In the presence of hypophosphite, the polyhedral morphology of the films was lost, although deposits were rich in cobalt, probably as a consequence of the P incorporation into the deposits. Rounded grains of nanometric size (60–100 nm; Fig. 6a) were observed. Nodular morphology was maintained by increasing deposition charge (Fig. 6b).

Deposits prepared galvanostatically present different morphology as a function of the current density applied as

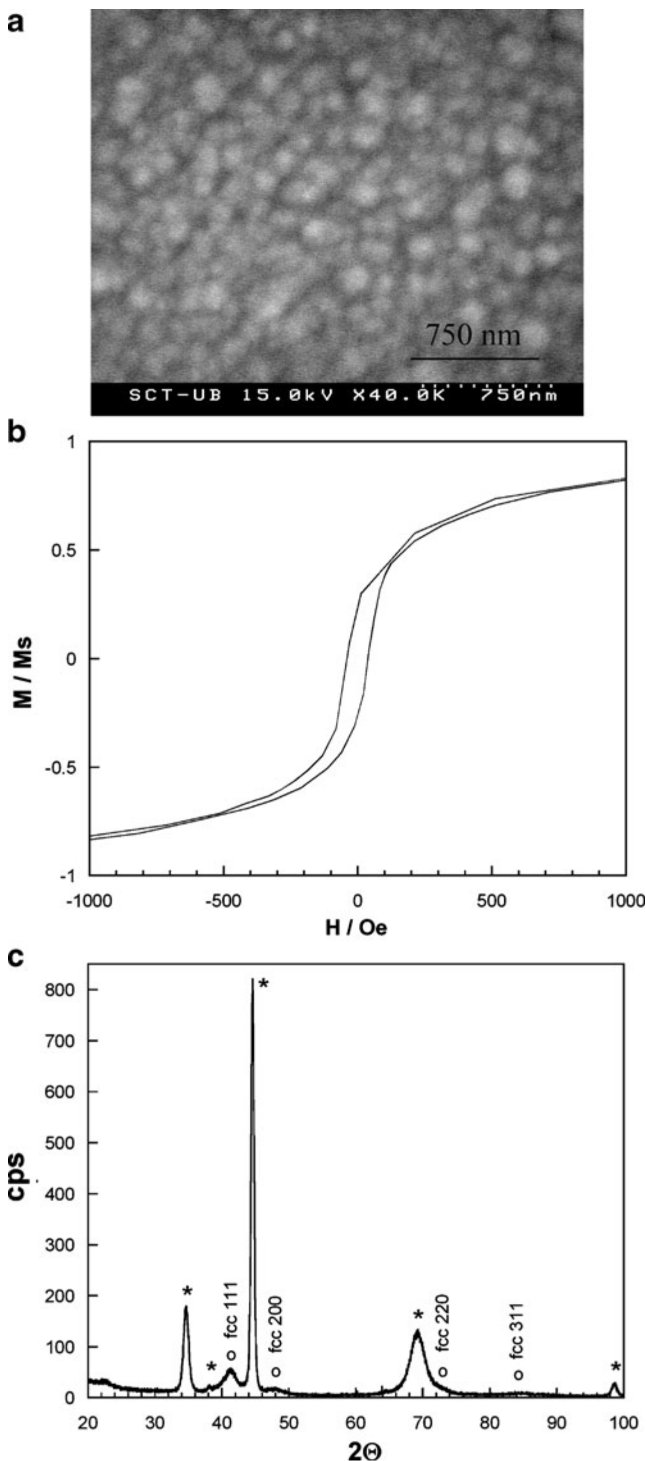

Fig. 4 **a** FE-SEM image of a CoPt deposit of 155 nm (sample A6), **b** normalized room temperature magnetization curve taken with the applied field parallel, and **c** X-ray diffractogram of the same deposit

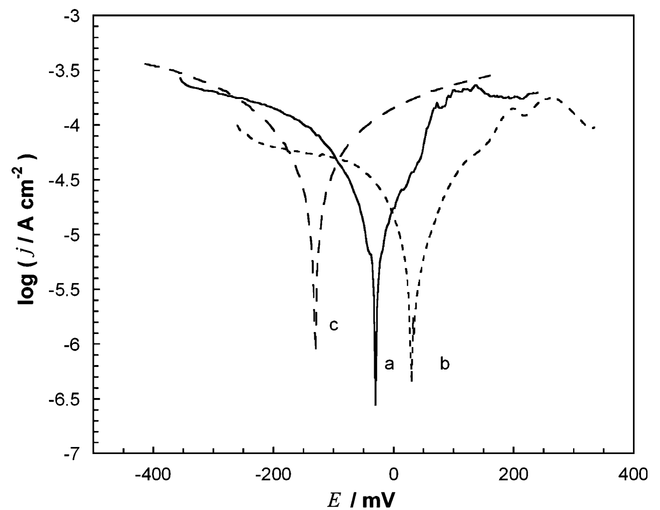

Fig. 5 Potentiodynamic polarization curves in logarithmic scale corresponding to CoPt deposits of around 120–150 nm. *a* Sample B1, hcp phase; *b* sample A1, hcp phase; *c* sample A6, fcc phase

it led to different stabilization potential (−690 mV at −4 mA cm^{-2} (Fig. 6c, d) and −900 mV at −25 mA cm^{-2} (Fig. 6e)): Low current densities led to coral-like no uniform deposits whereas more compact deposits were obtained by increasing current densities. In this case, cracked films were obtained that evolved to more compact and less cracked ones by increasing their thickness (Fig. 6f).

High coercivity values were obtained (Fig. 7a) for deposits containing P. Hard magnetic properties can be enhanced due to the segregation of P at grain boundaries, forming defects sites capable to behave as pinning sites against domain wall motion [36]. CoPtP deposits showed hcp structure (Fig. 7b) with Pt incorporation into the cobalt lattice, independently of the deposition technique used (potentiostatic or galvanostatic). Cell parameters for CoPtP deposits with 40 wt.% Pt were a=0.255 nm, c=0.418 nm, and V=0.0235 nm^3, lower than those obtained for pure-CoPt films as a consequence of the lower Pt incorporation. Then, high coercivities of the CoPt films containing phosphorous can be originated by the combination of the high magnetic anisotropy of the hexagonal phase and the presence of nonmagnetic precipitates that hinder domain wall motion. CoPtP deposits showing Pt percentages around 40 wt.% and some P incorporation showed the maximum coercivity (1,300–1,400 Oe), but lower permeability than pure CoPt deposits. The comparison of the magnetic properties of the films prepared at different deposition charges revealed similar magnetic behavior,

Table 2 Corrosion potentials (E_{corr}) and corrosion current densities (j_{corr}) of CoPt deposits

Crystalline structure	Co (wt.%)	Pt (wt.%)	E_{corr} (mV)	j_{corr} (μA cm^{-2})
hcp	60.9	39.1	−31	0.40
hcp	40.4	59.6	30	0.46
fcc	22.6	77.4	−130	0.68

Table 3 Composition of CoPtP deposits prepared at 40 °C in different conditions from 2.5×10^{-3}M $CoCl_2$+1.2×10^{-3}M Na_2PtCl_6+1 M NH_4Cl+30 g dm^{-3} H_3BO_3+10^{-2}M NaH_2PO_2 solution

Samples	$-E$ (mV)	$-j$ (mA cm^{-2})	Stirring (rpm)	$-Q$ (C cm^{-2})	wt.% Co	wt.% Pt	wt.% P
C1	950		60	20	58.0	38.7	3.3
C2	950		1,100	170	58.3	41.3	0.4
C3	950		1,100	290	74.5	25.4	0.1
C4		4	60	20	55.8	40.8	3.4
C5		25	60	20	52.0	45.2	2.8
C6		25	60	40	55.1	44.6	0.3

although at high deposition charges, the decrease of both platinum and phosphorous percentages may decrease the coercivity and increase the susceptibility of the deposit.

Corrosion resistance of CoPtP was analyzed and compared with that corresponding to CoPt deposits of similar Pt percentage and same structural phase (hcp; Fig. 8). Even in the presence of low P percentages in the deposits, a shift of the corrosion potential to more positive values was observed for CoPtP films respect to CoPt ones (120 mV for CoPtP and −31 mV for CoPt); the corrosion current

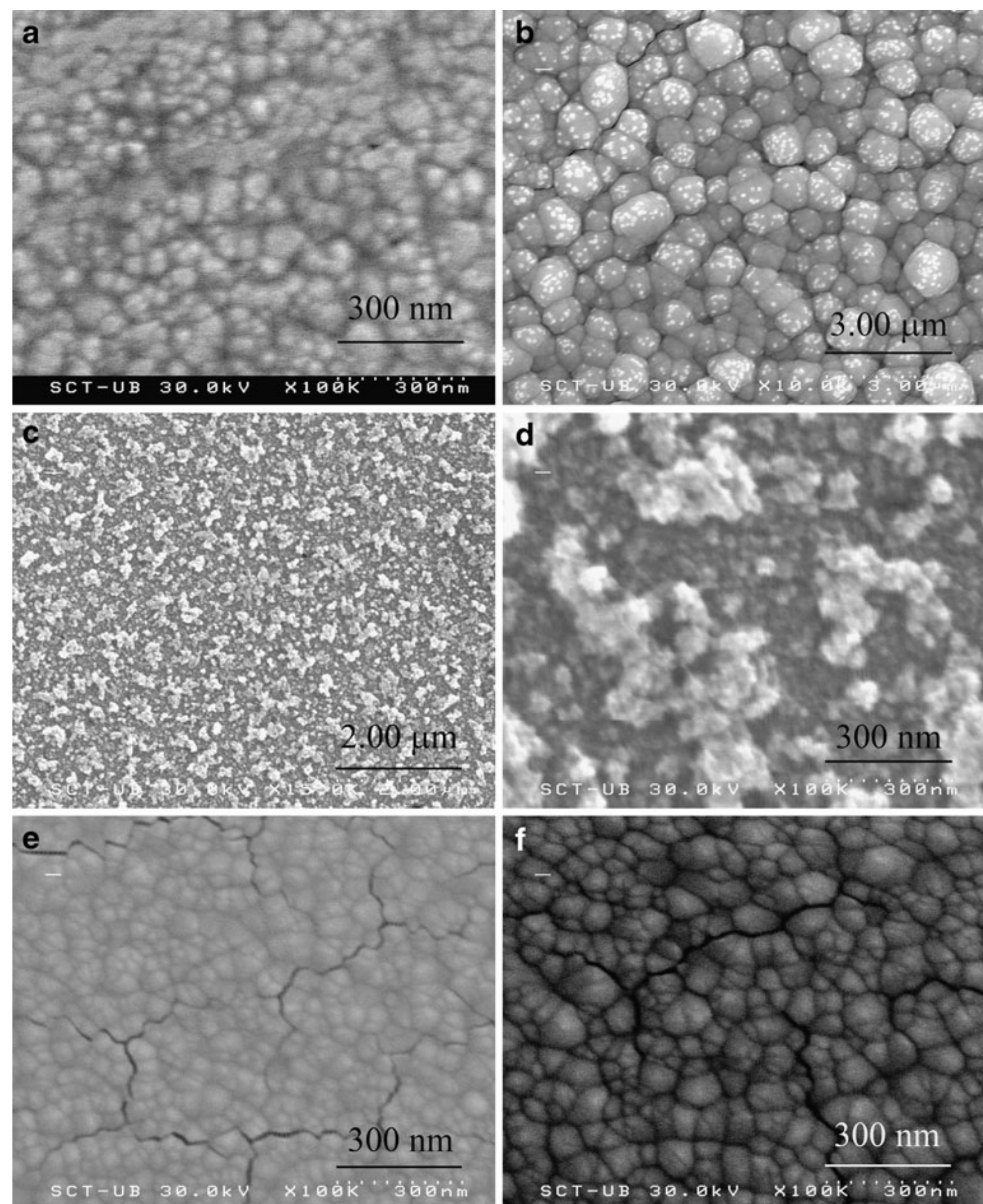

Fig. 6 FE-SEM images of different CoPtP deposits obtained from a 2.5×10^{-3}M $CoCl_2$+1.2×10^{-3}M Na_2PtCl_6+1 M NH_4Cl+30 gdm^{-3} H_3BO_3+10^{-2}M NaH_2PO_2 solution. **a** Sample C1, thickness 130 nm. **b** Sample C2, thickness 1.0 µm. **c**, **d** Sample C4, thickness 145 nm. **e** Sample C5, thickness 120 nm. **f** Sample C6, thickness 306 nm

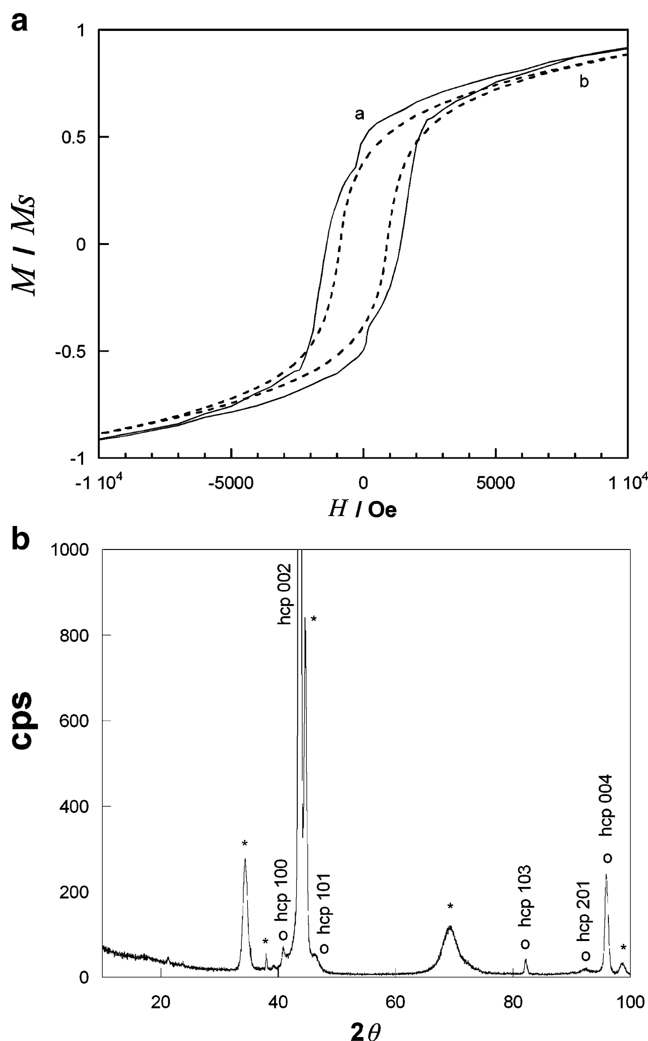

Fig. 7 **a** Normalized room temperature magnetization curves taken with the applied field parallel of CoPtP deposits. *a* Sample C1, thickness 130 nm; *b* sample C3, thickness 1.4 μm. **b** X-ray diffractogram of the deposit of sample C1

densities are lower for CoPtP (0.17 μA cm^{-2}) than for CoPt (0.40 μA cm^{-2}). The presence of P makes nobler the alloy respect to pure CoPt in a similar way that the phosphorous inclusion in some nanocrystalline metals as Ni or Co improves their corrosion resistance, even for low P percentages [37, 38]. The possible segregation of P in the grain boundaries or the enrichment of P on the surface seems to minimize the corrosion process of the alloy. Then, the incorporation of P in the deposits led to films with higher coercivity and better corrosion resistance properties.

Conclusions

It was possible to electrodeposit CoPt and CoPtP films of different thickness over silicon/seed layer. The presence of hypophosphite in the bath did not affect the deposition rate of the deposits. However, differences in the nucleation process were observed that entailed differences in the deposits compositions, limiting the Pt percentage in the deposits obtained from the bath containing hypophosphite. For CoPt deposits, it was possible to maintain a constant composition for different deposition charges, whereas for CoPtP deposits, the P and Pt percentages decrease by increasing deposition charge.

For pure-CoPt deposits, it was possible to control the films properties (morphology, crystalline structure, magnetic behavior, and corrosion resistance) as a function of the applied potential/current density and, as a consequence, of the films composition. Low deposition potentials (around −600 mV) led to CoPt films with a Pt percentage around 75 wt.%, nodular morphology, fcc structure, and low coercivity. More negative deposition potentials (around −950 mV) allowed obtaining CoPt films with Pt percentage up 65 wt.%, polyhedral fine grains, Co hcp structure distorted due to Pt incorporation, higher coercivity, tending to hard magnetic behavior, and better corrosion resistance. Nanocrystalline domains were present in both cases.

The presence of hypophosphite in the chloride bath induced the incorporation of low P percentages in the CoPt deposits but modified the magnetic and corrosion resistance properties of the films. Since the hypophosphite presence in the electrolytic bath tested limited the Pt incorporation, the more anisotropic hcp structure of the films was maintained and the formation of a Pt-rich fcc structure that presented worse hard magnetic and corrosion resistance properties was avoided. However, the presence of hypophosphite in the bath led to a change in the morphology of the deposits that evolved from polyhedral to nodular ones, although they were nanocrystalline in both cases. Hard magnetic behavior

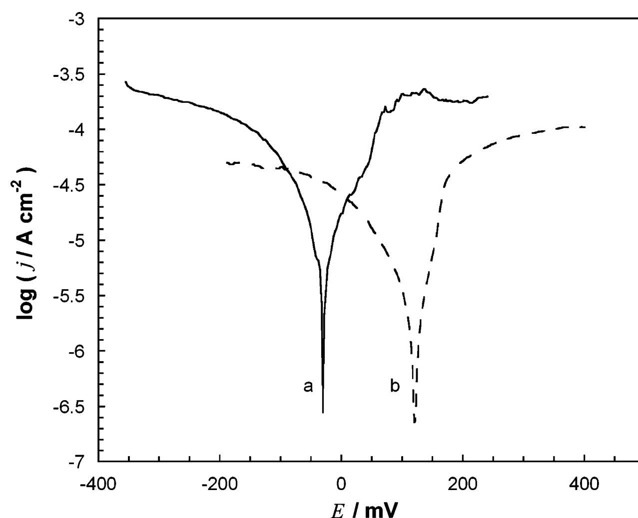

Fig. 8 Potentiodynamic polarization curves in logarithmic scale corresponding to *a* sample B1, thickness 140 nm, *b* sample C5, thickness 110 nm

and corrosion resistance were enhanced probably as a consequence of P segregation between the magnetic grains. The maximum coercivity value (1,400 Oe) was obtained from CoPtP deposits with Pt percentages of 40 wt.%. This entails profits because better coercivity values were obtained from CoPtP films with 40 wt.% than CoPt films with high Pt percentages (60 wt.%), being more economic the preparation process. The P incorporation also improves the corrosion resistance of the deposit. So these deposits are promising layers to be incorporated in magnetic MEMS devices.

Acknowledgments The authors wish to thank the Serveis Cientificotècnics (Universitat de Barcelona) and the Servei de Magnetoquímica (Universitat de Barcelona) for the use of their equipment. This paper was supported by contract MAT2006-12913-C02-01 from the Comisión Interministerial de Ciencia y Tecnología (CICYT).

References

1. Casals-Terré J, Duch M, Plaza JA, Esteve J, Pérez-Castillejos R, Vallés E, Gómez E (2008) Sens Actuators, A, Phys 147:600
2. Osaka T, Sawaguchi T, Mizutani F, Yokoshima T, Takai M, Okinaka Y (1999) J Electrochem Soc 146:3295
3. Tabakovic I, Inturi V, Riemer S (2002) J Electrochem Soc 149: C18
4. Lallemand F, Comte D, Ricq L, Renaux P, Pagetti J, Dieppedale C, Gaud P (2004) Appl Surf Sci 225:59
5. Chin TS (2000) J Magn Magn Mater 209:75
6. Cho HJ, Ahn CH (2002) J Microelectromechanical Syst 11:78
7. Park DY, Myung NV, Schwartz M, Nobe K (2002) Electrochim Acta 47:2893
8. Myung NV, Park DY, Yoo BY, Sumodjo PTA (2003) J Magn Magn Mater 265:189
9. Niarchos D (2003) Sens Actuators A Phys 109:166
10. Guan S, Nelson BJ (2005) Sens Actuators A Phys 118:307
11. Guan S, Nelson BJ (2005) J Magn Magn Mater 292:49
12. Su Y, Wang H, Ding G, Cui F, Zhang W, Chen W (2005) IEEE Trans Magn 41:4380
13. Pigazo F, Palomares FL, Cebollada F, González JM (2008) J Magn Magn Mater 320:1966
14. Lew KS, Rajab M, Thanikaikarasan S, Kim T, Kim YD, Mahalingam T (2008) Mater Chem Phys 112:249
15. Pané S, Gómez E, Vallés E (2007) Electrochem Commun 9:1755
16. Xu QY, Kageyama Y, Suzuki T (2005) J Appl Phys 97:10K308
17. Chen XY, Jiang ZhL, Zhang L, Chen Y, Bai FM, Chen HM, Zhu J (2003) Mater Sci Forum 426:2381
18. Liu Y, Dallimore MP, McCormick PG, Alonso T (1992) Appl Phys Lett 60:3186
19. Pattanaik G, Kirkwood DM, Xu X, Zangari G (2007) Electrochim Acta 52:2755
20. Myung NY, Park DY, Schwartz M, Nobe K, Yang H, Yang CK, Judy JW (2000) Magnetic materials, processes and devices. In: Krongelb S, Romankiw LT, Ahn CH, Chang JW, Schwarzacher W (eds) The electrochemical society proceedings series. Electrochemical Society, Pennington
21. Zuzek-Rozman K, Krause A, Leistner K, Fähler S, Schultz L, Schlorb H (2007) J Magn Magn Mater 314:116
22. Cavallotti PL, Bestetti M, Franz S (2003) Electrochim Acta 48:3013
23. Zana I, Zangari G, Park JW, Allen MG (2004) J Magn Magn Mater 272–276:e1775
24. Lee KH, Kang SW, Kim GH, Jeung WY (2004) J Magn Magn Mater 272–276:e925
25. Park HD, Lee KH, Kim GH, Jeung WY (2006) J Appl Phys 99:08N305
26. Vieux-Rochaz L, Dieppedale C, Desloges B, Gamet D, Barragatti C, Rostaing H, Meunier-Carus J (2006) J Micromech Microeng 16:219
27. Cortés M, Matencio S, Gómez E, Vallés E (2009) J Electroanal Chem 627:69
28. Oliveira MC, do Rego AMB (2006) J Alloys Compd 425:64
29. Dulal SMSI, Kim TH, Shin CB, Kim CK (2008) J Alloys Compd 461:382
30. Cheonga WJ, Luana BL, Shoesmitha DW (2004) Appl Surf Sci 229:282
31. Homma T, Komatsu I, Tamaki A, Nakai H, Osaka T (2001) Electrochim Acta 47:47
32. Gómez E, Vallés E (2002) J Appl Electrochem 32:693
33. Boultif A, Loüer D (2004) J Appl Crystallogr 37:724
34. Cullity BD (1978) Elements of X-ray diffraction, 2nd edn. Addison-Wesley, Boston
35. García-Torres J, Gómez E, Vallés E (2009) J Appl Electrochem 39:233
36. Homma T, Sezai Y, Osaka T, Maeda Y, Donnet DM (1997) J Magn Magn Mater 173:314
37. Burchardt T, Hansen V, Valand T (2001) Electrochim Acta 46:2761
38. Jung H, Alfantazi A (2006) Electrochim Acta 51:1806